non peer-reviewed preprint

The highly nonlinear viscosity of fast-flowing glacier ice

Meghana Ranganathan[1,2*] and Brent Minchew[1]

[1]Department of Earth, Atmospheric and Planetary Sciences,
Massachusetts Institute of Technology, Cambridge, MA, USA
[2]School of Earth and Atmospheric Sciences,
Georgia Institute of Technology, Atlanta, GA, USA

*To whom correspondence should be addressed:
Meghana Ranganathan (meghanar@ucar.edu)

Glacier flow modulates sea level and is governed by the viscous deformation of ice. Multiple molecular-scale mechanisms facilitate viscous deformation, but it remains unclear how each contributes to glacier-scale deformation and how to represent them in ice-flow models. Here, we present a model of ice deformation that unifies existing estimates of the viscous parameters and provides a framework for estimating their values. We infer from observations the dominant deformation mechanisms in the Antarctic Ice Sheet, showing that, contrary to long-standing assumptions, dislocation creep, with viscous stress exponent $n = 4$, likely dominates in all fast-flowing areas. This increase from the canonical $n = 3$ changes the stability portrait of marine ice sheets by reducing the likelihood of unstable steady-state configurations on reverse bed slopes under given climate conditions.

Most mass loss from the Antarctic Ice Sheet (AIS) occurs through fast-flowing glaciers and ice streams (*1–4*), which transport ice from the grounded ice sheet to the ocean. Changes in mass loss rates from AIS form the largest sources of uncertainty in projections of sea-level rise and the response of AIS to climate change. These changes in mass loss are governed by rates of ice deformation (*5*). Therefore understanding and modeling the mechanisms that govern ice deformation – among the oldest, most enduring, and most fundational questions in glaciology – is necessary for understanding the evolution of AIS and other glaciated areas, reliably projecting sea-level rise, and quantifying the associated uncertainties.

Based on experimental results and our understanding of polycrystalline materials, ice deformation can be modeled by a composite flow law (*6, 7*), which gives the total (bulk) deformation rate $\dot{\epsilon}$ as the sum of deformation rates from different deformation mechanisms. Four primary deformation mechanisms have been identified in ice. Diffusion creep $\dot{\epsilon}_{\text{diff}}$ arises from the diffusion of vacancies in the crystalline lattice. Grain-boundary sliding $\dot{\epsilon}_{\text{gbs}}$ involves the deformation of a lattice in which the movement occurs within grain boundaries. Dislocation creep $\dot{\epsilon}_{\text{dis}}$ entails the motion of defects (dislocations) in the crystalline lattice. Basal sliding $\dot{\epsilon}_{\text{basal}}$ encompasses slip along the basal planes of crystals to accommodate grain-boundary sliding. Most of these mechanisms act in parallel but the two grain boundary sliding mechanisms, $\dot{\epsilon}_{\text{gbs}}$ and $\dot{\epsilon}_{\text{basal}}$, act in series because they have opposing rate-limiting mechanisms. Thus, the total rate of deformation, as presented in (*7*), is

$$\dot{\epsilon} = \dot{\epsilon}_{\text{diff}} + \left[\frac{1}{\dot{\epsilon}_{\text{basal}}} + \frac{1}{\dot{\epsilon}_{\text{gbs}}}\right]^{-1} + \dot{\epsilon}_{\text{dis}} \tag{1}$$

where each term on the righthand side can be modeled with a power-law relation of the form $\dot{\epsilon}_i = A_i(T, d)\tau^{n_i}$, with T representing ice temperature, d the mean grain size, τ deviatoric stress, and the parameters A_i and n_i the flow-rate parameter and stress exponent, respectively, for the i^{th} deformation mechanism.

Rather than trying to represent each individual mechanism as in Eq. 1, ice sheet models generally incorporate a single power-law relation commonly known as Glen's Flow Law, which defines a relationship between the effective strain rate $\dot{\epsilon}_e$ and effective deviatoric stress τ_e (second invariants of their respective tensors) such that

$$\dot{\epsilon}_e = A\tau_e^n \tag{2}$$

While the simplicity of Glen's Law is attractive for modeling, uncertainties in the values of A and n arise from the complex rheology of ice (illustrated in Eq. 1) and challenges in calibrating these parameters at scale in natural glacier ice. In particular, lacking a formal parameterization that captures deformational processes and their effects on A and n, ice sheet modelers must use an assumed value of n and a value of A calibrated from sparse observations for the assumed n (*8–11*). By far the most common assumption is $n = 3$ as a constant value for all ice flow conditions and all model timesteps. But while the value of $n = 3$ agrees with some studies (e.g. (*9*)), other studies have inferred values between 1 and 5 based on laboratory experiments (*7, 12–14*), in-situ measurements (*9, 15*), observational studies (*16–18*), and computational methods (*19, 20*).

The assumed values of n and A in ice-flow models have substantial yet largely unexplored implications for ice sheet and sea-level rise projections because n is the exponent that governs the sensitivity of viscosity to stress, and viscosity is of paramount importance to viscous ice flow (*23*). In particular, these parameters have profound effects on our conceptualization of the stability of marine ice sheets, like the West Antarctic Ice Sheet, the largest contributor to uncertainties in projections of sea-level rise (*24*) (Figure 1). Marine ice sheets have beds that are well below sea level and are thought to be unstable when the bed deepens inland (a retrograde slope) because ice floats, allowing for a bouyancy-driven feedback, known as the marine ice sheet instability (MISI), that can cause rapid retreat of the ice sheet (*21, 22, 25, 26*).

Here, we apply a simple, steady-state model (*22*) to a commonly used idealized marine

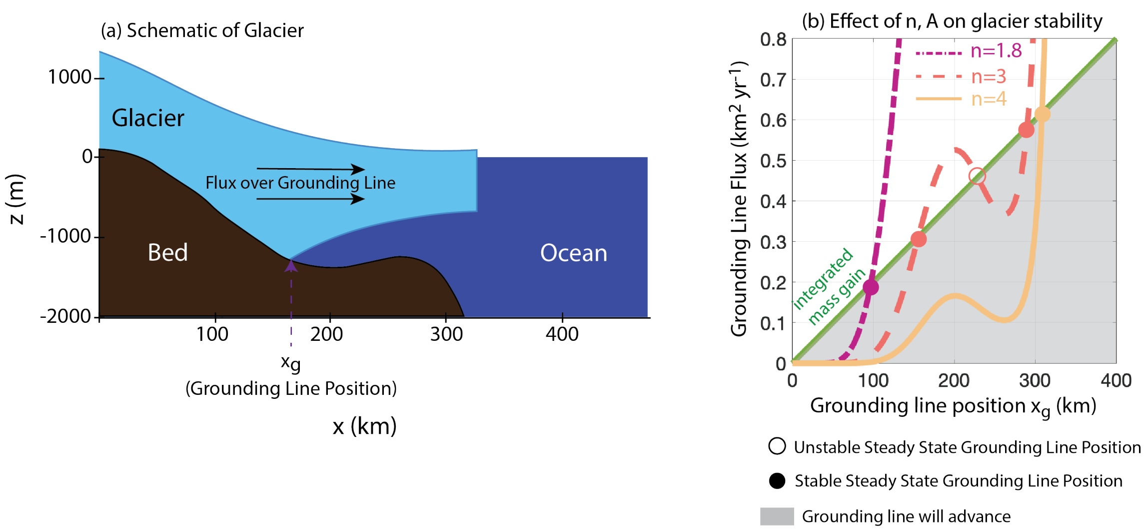

Figure 1: **Effect of n, A on grounding line flux:** (a) Schematic of a marine ice sheet, denoting the grounding line position and the flux of ice over the grounding line and into the ocean, a value that affects the mass loss from grounded portions of the ice sheet. The bed geometry is defined in (*21*). (b) Estimates of the modeled (*22*) grounding line position (x-axis) and grounding line flux for $n = 2, 3, 4$. Intersections of the green, diagonal line (showing mass flux from surface accumulation integrated over the upstream catchment) with the flux curves are the steady-state grounding line positions, with solid and open circles indicating stable and unstable configurations, respectively. Grey background denotes where the grounding line will advance, and white background denotes where the grounding line will retreat.

ice sheet geometry (Fig. 1a) to explore how changing the values of n, and correspondly A, influences the potential for MISI under given climate conditions (Fig. 1b, solid green line). By definition, MISI can be triggered when the combination of ice rheology and climate allows for an unstable steady state when the grounding line (boundary between grounded and floating ice) is on a retrograde bed slope (Fig. 1b, orange dashed curve). Our results for $n = 2, 3, 4$ (Fig. 1b) show that varying the viscous parameters within the range of accepted values changes the relationship between ice mass flux from land to the ocean (a.k.a., grounding line flux) and grounding line position enough to introduce or eliminate the potential for MISI under given climate scenarios. For the chosen climate scenario, there is an unstable grounding line position on the retrograde bed when $n = 3$, but for $n = 2$ and $n = 4$, the grounding line positions are unconditionally stable in the model (Fig. 1b, colored curves). There are no climate scenarios where a marine ice sheet has an unstable grounding line position for any A, n pair. This analysis shows that values of n and A are crucial for our estimates of marine ice sheet stability, and therefore projections of sea-level rise.

This need for more accurate and physically justified estimates of A and n in natural glacier ice motivates this study, wherein we present a model for ice deformation that represents the known mechanisms of deformation (Equation 1) and the couplings between ice rheology, temperature, and grain size. Based primarily on laboratory experiments (*6,7,27*), the typical stresses and temperature conditions in ice sheets reduce Eq. 1 to the sum of two mechanisms, dislocation creep $\dot{\epsilon}_{\mathrm{dis}}$ and grain boundary sliding $\dot{\epsilon}_{\mathrm{gbs}}$, so that $\dot{\epsilon}_e = \dot{\epsilon}_{\mathrm{dis}} + \dot{\epsilon}_{\mathrm{gbs}}$, where each term can be expanded such that $\dot{\epsilon}_{\mathrm{dis}} = A_{\mathrm{dis}}(T)\tau_e^4$ and $\dot{\epsilon}_{\mathrm{gbs}} = A_{\mathrm{gbs}}(T)d^{-1.4}\tau_e^{1.8}$. To represent the dependence of deformation rate on ice temperature and grain size, the two variables that affect the dominance of the deformation mechanisms, we couple Equation 1 to a thermomechanical model (*28*) and a steady-state grain size model (*29*), as discussed in (*30*). This allows us to constrain the mechanisms of ice deformation in natural glacier ice and estimate the viscous properties of ice for the full range of temperatures and stresses found in terrestrial glaciers and ice sheets.

Using this coupled model, we estimate the stress exponent n in Glen's Flow Law (Eq. 2) as a function of ice temperature and stress (Fig. 2a). We use creep activation energies from (*30*), which were calibrated using observations of n in the extensional regions of Antarctic ice shelves (*18*). Our results show that dislocation creep ($n = 4$) dominates when stresses are above 100 kPa, while grain boundary sliding ($n = 1.8$) dominates at lower stresses ($<$ 10 kPa), as expected from previous studies (*6, 7, 27, 31*). At intermediate stresses of order 10–100 kPa, a range that encompasses most values of stress found in fast-flowing areas of Antarctica, the dominant creep mechanism depends strongly on temperature, with dislocation creep ($n = 4$) dominating at warmer temperatures ($-10 < T \leq 0$ °C), which are expected in rapidly deforming areas (*32*), and multiple deformation mechanisms acting in concert at colder temperatures. At stresses below 30 kPa and temperatures colder than -10 °C, the estimated value of n is anomalously large due to elevated grain sizes; we do not expect these results to be realistic nor to impact the primary conclusions of this study because at such low stresses and temperatures, other deformation mechanisms unlikely to play important roles in fast-flowing glaciers and not sufficiently represented in the model (such as basal slip or diffusion creep) may be active.

Our model provides a unifying framework for ice viscosity that explains the variations in observational studies from $n \approx 2$ to $n \approx 4$ as a manifestation of measurements being taken at various stresses and ice temperatures. To illustrate the agreement between our model and observations, we highlight the results of some observational studies with semi-transparent boxes in Fig. 2a. Many of the studies concluding $n = 2 - 3$ were done in conditions that fall along the boundary between $n \approx 2$ and $n = 4$, with stresses of $10 - 100$ kPa and temperatures < -10 °C (e.g. Devon Island Ice Cap, Canada (RP88) (*35*), and Byrd Station, Antarctica, and Camp Century, Greenland (P83) (*34*)). Studies conducted at Taylor Glacier, Antarctica (CK11) (*37*),

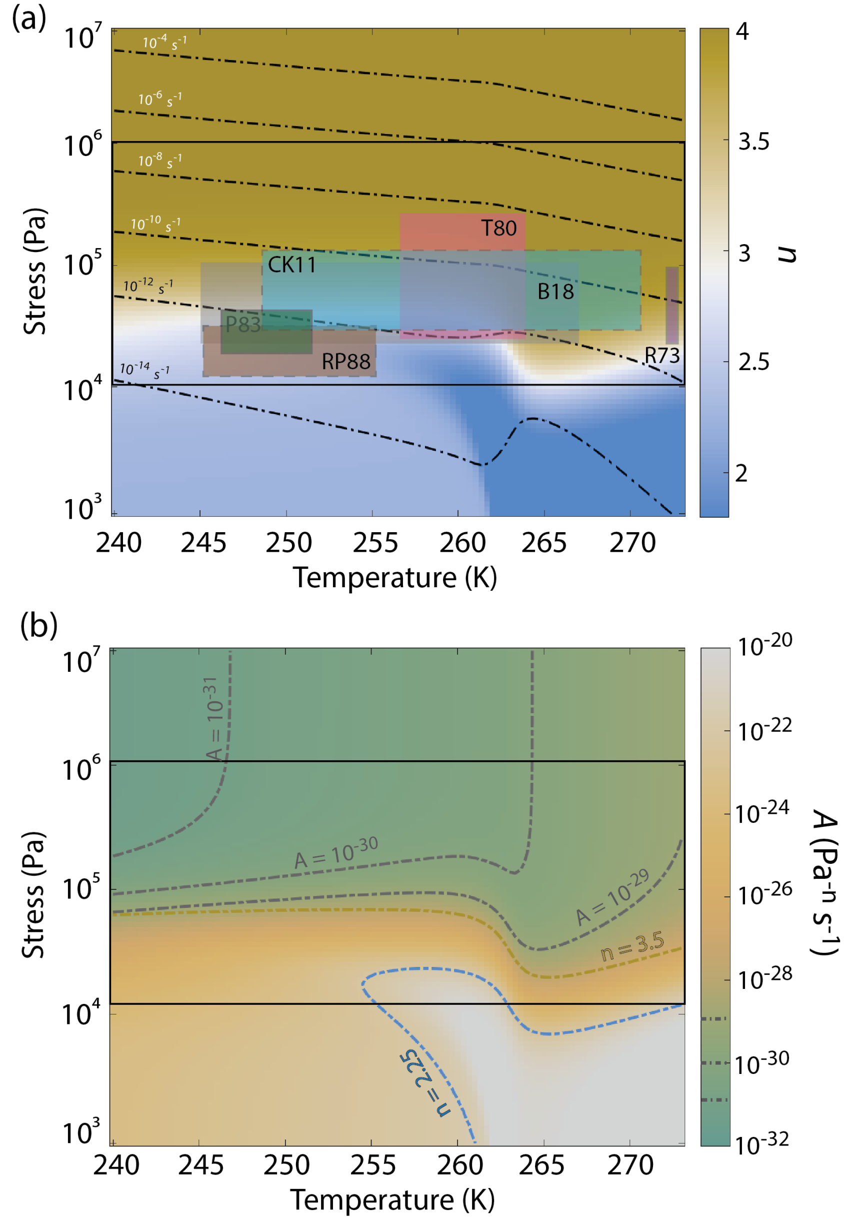

Figure 2: Estimating $\mathbf{n}$ and $\mathbf{A}$ for varying flow conditions: We estimate for varying stresses and ice temperatures common in naturally-deforming glacier ice: (a) stress exponent in Glen's Flow Law n from our model compared to observational studies, with outlines denoting confidence in the ranges (solid outlines - explicit uncertainties were given in the original study, dashed outlines - enough information was provided in the original study to suggest ranges, no outlines - ranges were inferred by us based on information provided in the original study and knowledge of regions). The labels, which represent author lastname and year of publication, and inferred n values are: R73 (*33*) $n = 4.2$, P83 (*34*) $n = 2.5 - 3$, RP88 (*35*) $n = 2.9$, T80 (*36*) ($n = 3 - 4$), CK11 (*37*) $n = 3 - 4$, B18 (*17*) $n = 4.1$. (b) The flow-rate parameter in Glen's Flow Law A from Equation 2. Contour lines of (a-d) show values of constant strain-rate and red dots show the ice temperatures computed from stress by a thermomechanical model. Contour lines show values of $n = 2.25$ (blue), $n = 3.5$ (gold) and values of A (grey).

and Roosevelt Island, Antarctica (T80) (*36*), concluded that n may vary between $n = 3$ and $n = 4$. These two studies considered higher stresses and a wider range of ice temperatures, falling between the boundary of $n = 3$ and $n = 4$ in our deformation map (Fig. 2a). Our estimates are also compatible with studies that conclude $n = 4$, including in temperate ice (R73) (*33*), where we also estimate $n = 4$. Finally, $n \approx 4$ has been inferred in the northern part of the Greenland Ice Sheet (B18), where stresses are $\sim 50 - 100$ kPa (*17*). Based on estimates of what the ice temperatures may be in these regions, we estimate $n = 3 - 4$ for the same flow conditions.

Applying our estimates of n to Glen's Flow Law, we calculate the prefactor A (Fig. 2b). In regions where $n \approx 4$, we estimate $A \leq 10^{-28}$ $\mathrm{Pa^{-n}\ s^{-1}}$, while where $n \approx 2$, $A > 10^{-20}$ $\mathrm{Pa^{-n}}$ $\mathrm{s^{-1}}$. Given the difference in exponent, the increase in the magnitude of A for decreasing n is expected. A is temperature- and grain size-dependent, and therefore as temperature increases, A increases approximately one and a half orders of magnitude. Using this method and with reasonable estimates of n, strain-rate, and applied stress, we can estimate ice viscosity in ice sheets, providing insight into the magnitude of ice softening due to mechanisms such as fabric development, heating, recrystallization, and liquid water content.

Our model demonstrates how fundamental rheological parameters are affected by ice flow conditions, and it enables estimates of the dominant deformation mechanisms and relevant viscous parameters across AIS. This is possible because ice in Antarctica should be relatively dry; ultimately we will be able to apply the model to wetter ice in Greenland once we better understand how intersticial liquid water content influences the balance of creep mechanisms. Here, we present estimates in AIS with specific focus on Pine Island Glacier, Byrd Glacier, Bindschadler and MacAyeal Ice Streams, and Amery Ice Shelf, all of which are well-observed, fast-flowing areas that represent a range of dynamical characteristics. Computing n, A requires observations of effective strain-rates, ice thickness, and surface mass balance. Effective strain-rates are derived from Landsat 7 and 8 velocity fields (*2*) using methods described in (*28*). Ice thickness is calculated from basal topography from BedMachine (*38*) and surface elevation from the Reference Elevation Model of Antarctica (*39*). Surface mass balance, averaged over 1979-2019, is estimated from RACMO, a regional climate model (*40*). The estimates presented here are depth-averaged.

We estimate $n \approx 4$ in all fast-flowing areas of AIS (Fig. 3). Within ice streams, the value of n varies slightly around $n = 4$. For example, within Byrd Glacier, the value in the centerline is ~ 3.9. The value of n varies between 3.9 and 4 near the grounding line of Bindschadler and MacAyeal Ice Streams. However, this variance is minimal and $n = 4$ is a good approximation over all of these ice streams.

We further present estimates of A across the AIS and in specific regions of the ice sheet. In Antarctic ice streams, lateral shear is primarily localized in the lateral margins, and thus in our model the margins of ice streams are warmer and expected to have larger grain sizes (*29*). Both of these processes affect estimates of ice viscosity. Here, we see generally that A is larger in these rapidly-deforming regions of the ice sheet. This supports a number of modeling and computational studies suggesting that ice is warmer and softer in shear margins (*43–48*).

Ultimately, the model representation of ice flow likely has significant effect on projections of glacier behavior and ice sheet stability (Fig. 1). Our model provides physically-informed estimates of the fundamental parameters underlying our representation of viscous ice flow. The practical implications of our model are 1) the unification of ice deformation that captures and contextualizes the range of existing estimates of the stress exponent n and 2) establishment of a framework for estimating the values of A and n in Glen's Flow Law (Eq. 2) based on first principles, laboratory experiments, and observations. This modeling framework can be readily applied to existing ice-flow models while respecting the various coupled physical processes, such as internal heating due to deformation and evolving grain sizes, as a way of improving our

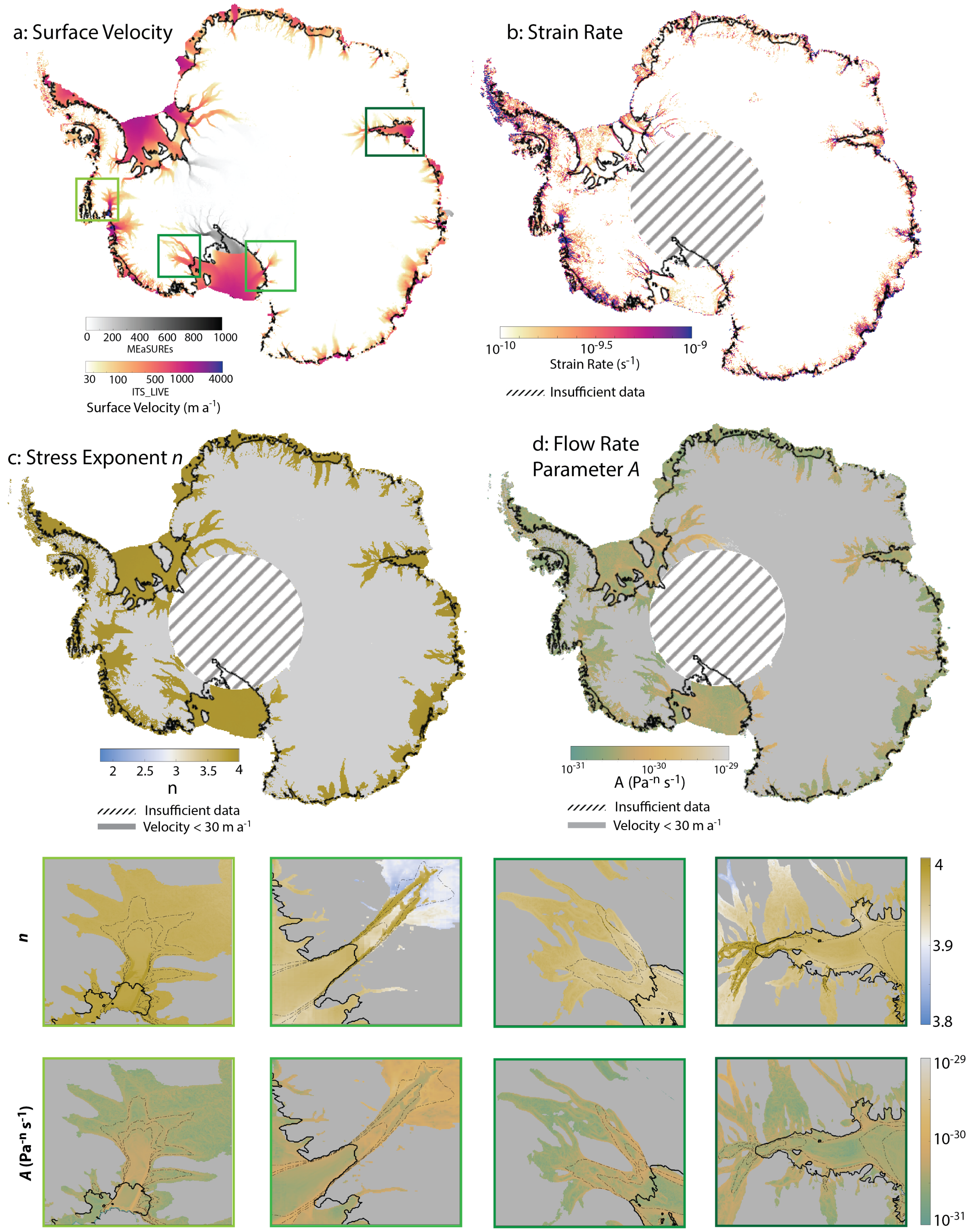

Figure 3: Estimating $\mathbf{n}$ and $\mathbf{A}$ in regions of the Antarctic Ice Sheet: Using observations of (a) surface velocity (*2, 3*) and (b) calculated strain-rates (*41*), we estimate (c) n and (d) A over the Antarctic Ice Sheet. Cross-hatching shows gaps in the data, and greyed out regions are where measured velocity is less than 30 m a^{-1}, and our model is not applicable. In the bottom two rows, we show n (upper row) and A (lower row) in (left to right) Pine Island Glacier, Byrd Glacier, Bindschadler and MacAyeal Ice Streams, and the Amery Ice Shelf. Dashed lines denote surface velocity contours of 200 m yr^{-1}, 400 m yr^{-1}, 600 m yr^{-1}. Solid lines denote the grounding line from Bedmap2 (*42*).

parameterization of ice deformation and as part of a broader community effort to make more reliable projections of future sea-level rise.

Acknowledgements

The authors benefited greatly from discussions with Joanna Millstein, David Goldsby, Colin R. Meyer, Jerome Neufeld. The authors also thank Marianne Haseloff for providing the code for the ice sheet stability model, and for providing the information for running the model. **Funding:** M.I.R. was supported by the School of Science Service Fellowship, Martin Fellowship, NSFGEO-NERC award 1853918, NEC Corporation Fund for Research in Computers and Communications, and the NOAA Climate Global Change postdoctoral fellowship. B.M. acknowledges funding from NSFGEO-NERC award 1853918, NSF-NERC award 1739031, and NEC Corporation Fund for Research in Computers and Communications. **Author Contributions:** Both authors conceived of the study and contributed to the model development. M.I.R. performed the experimentation and developed the figures. Both authors contributed to analyzing and interpreting the results. M.I.R. wrote the original draft and both authors revised and edited the final draft. **Competing interests:** The authors declare no competing interests. **Data and materials availability:** The source code for the model presented in this study are openly available at https://github.com/megr090/DeformationMechanisms. No new data were produced for this study, and data used in this study are publicly available through their respective publications.

References

1. E. Rignot, J. Mouginot, B. Scheuchl, *Science* **333**, 1427 (2011).
2. A. S. Gardner, *et al.*, *The Cryosphere* **12**, 521 (2018).
3. J. Mouginot, E. Rignot, B. Scheuchl, *Geophysical Research Letters* **46**, 9710 (2019).
4. J. De Rydt, R. Reese, F. S. Paolo, G. H. Gudmundsson, *The Cryosphere* **15**, 113 (2021).
5. K. M. Cuffey, *Glacier Science and Environmental Change*, P. G. Knight, ed. (Blackwell Science Ltd, 2006), pp. 290–300.
6. D. L. Goldsby, D. L. Kohlstedt, *Lunar and Planetary Science* (1997).
7. D. L. Goldsby, D. L. Kohlstedt, *Journal of Geophysical Research: Solid Earth* **106**, 11017 (2001).
8. R. H. Thomas, *Journal of Glaciology* **12**, 55 (1973).
9. K. Jezek, R. Alley, Thomas, *Science* **227**, 1335 (1985).
10. W. Budd, T. Jacka, *Cold Regions Science and Technology* **16**, 107 (1989).
11. K. Cuffey, W. Paterson, *The Physics of Glaciers* (Elsevier, 2010), fourth edn.
12. J. Glen, *Proceedings of the Royal Society of London. Series A. Mathematical and Physical Sciences* **228**, 519 (1955).
13. P. Barnes, D. Tabor, J. C. F. Walker, *Proceedings of the Royal Society of London. A. Mathematical and Physical Sciences* **324**, 127 (1971).
14. C. J. C. Adams, N. R. Iverson, C. Helanow, L. K. Zoet, C. E. Bate, *Frontiers in Earth Science* **9**, 1 (2021).

15. J. Nye, *Proceedings of the Royal Society of London. Series A. Mathematical and Physical Sciences* **239**, 113 (1957).

16. F. Gillet-Chaulet, R. C. Hindmarsh, H. F. Corr, E. C. King, A. Jenkins, *Geophysical Research Letters* **38**, 1 (2011).

17. P. D. Bons, *et al.*, *Geophysical Research Letters* **45**, 6542 (2018).

18. J. D. Millstein, B. M. Minchew, S. S. Pegler, *Communications Earth Environment* **3**, 1 (2022).

19. V. Rommelaere, D. R. Macayeal, *Annals of Glaciology* pp. 43–48 (1997).

20. E. Larour, *Geophysical Research Letters* **32**, L05503 (2005).

21. C. Schoof, *Journal of Geophysical Research* **112**, F03S28 (2007).

22. M. Haseloff, O. V. Sergienko, *Journal of Glaciology* pp. 1–18 (2022).

23. M. Zeitz, A. Levermann, R. Winkelmann, *Cryosphere* **14**, 3537 (2020).

24. B. Fox-Kemper, *et al.*, *Climate Change 2021: The Physical Science Basis. Contribution of Working Group I to the Sixth Assessment Report of the Intergovernmental Panel on Climate ChangeScience Basis. Contribution of Working Group I to the Sixth Assessment Report of the Intergover* **2018**, 1 (2021).

25. J. Weertman, *Journal of Glaciology* **13**, 3 (1974).

26. I. Joughin, B. E. Smith, B. Medley, *Science* **344**, 735 (2014).

27. D. Goldsby, D. Kohlstedt, *Scripta Materialia* **37**, 1399 (1997).

28. C. R. Meyer, B. M. Minchew, *Earth and Planetary Science Letters* **498**, 17 (2018).

29. M. Ranganathan, B. Minchew, C. R. Meyer, M. Peč, *Earth and Planetary Science Letters* **576**, 117219 (2021).

30. M. Ranganathan, B. Minchew, *EarthArXiV* (2022).

31. E. C. Pettit, E. D. Waddington, *Journal of Glaciology* **49**, 359 (2003).

32. C. R. Meyer, A. Yehya, B. Minchew, J. R. Rice, *Journal of Geophysical Research: Earth Surface* **123**, 1682 (2018).

33. C. F. Raymond, *Journal of Glaciology* **12**, 19 (1973).

34. W. S. B. Paterson, *Cold Regions Science and Technology* **8**, 165 (1983).

35. N. Reeh, W. S. Paterson, *Journal of Glaciology* **34**, 55 (1988).

36. R. H. Thomas, D. R. MacAyeal, C. R. Bentley, J. L. Clapp, *Journal of Glaciology* **25**, 47 (1980).

37. K. M. Cuffey, J. L. Kavanaugh, *Geology* **39**, 1027 (2011).

38. M. Morlighem, *et al.*, *Nature Geoscience* **13**, 132 (2020).

39. I. M. Howat, C. Porter, B. E. Smith, M.-J. Noh, P. Morin, *The Cryosphere* **13**, 665 (2019).

40. J. M. Van Wessem, *et al.*, *Journal of Glaciology* **60**, 761 (2014).

41. B. M. Minchew, M. Simons, B. Riel, P. Milillo, *Journal of Geophysical Research: Earth Surface* **122**, 167 (2017).

42. P. Fretwell, *et al.*, *The Cryosphere* **7**, 375 (2013).

43. H. P. Jacobson, C. F. Raymond, *Journal of Geophysical Research: Solid Earth* **103**, 12111 (1998).

44. W. D. Harrison, K. A. Echelmeyer, C. F. Larsen, *Journal of Glaciology* **44**, 615 (1998).

45. C. Schoof, *Journal of Glaciology* **50**, 208 (2004).

46. J. Suckale, J. D. Platt, T. Perol, J. R. Rice, *Journal of Geophysical Research: Earth Surface* **119**, 1004 (2014).

47. M. Ranganathan, B. Minchew, C. R. Meyer, G. H. Gudmundsson, *Journal of Glaciology* **67**, 229 (2021).

48. P. Hunter, C. Meyer, B. Minchew, M. Haseloff, A. Rempel, *Journal of Glaciology* pp. 1–15 (2021).

49. D. R. MacAyeal, R. A. Bindschadler, T. A. Scambos, *Journal of Glaciology* **41**, 247 (1995).

50. I. Joughin, D. R. MacAyeal, S. Tulaczyk, *Journal of Geophysical Research: Solid Earth* **109**, n/a (2004).

51. M. Morlighem, H. Seroussi, E. Larour, E. Rignot, *Journal of Geophysical Research: Earth Surface* **118**, 1746 (2013).

52. P. Duval, L. Arnaud, O. Brissaud, M. Montagnat, S. de la Chapelle, *Annals of Glaciology* **30**, 83 (2000).

53. P. Duval, M. Montagnat, *Journal of Geophysical Research: Solid Earth* **107**, ECV 4 (2002).

54. C. J. Wilson, Y. Zhang, *Annals of Glaciology* **23**, 293 (1996).

55. E. C. Pettit, T. Thorsteinsson, H. P. Jacobson, E. D. Waddington, *Journal of Glaciology* **53**, 277 (2007).

56. Y. Ma, *et al.*, *Journal of Glaciology* **56**, 805 (2010).

57. T. Chauve, M. Montagnat, P. Vacher, *Acta Materialia* **101**, 116 (2015).

58. B. M. Minchew, C. R. Meyer, A. A. Robel, G. H. Gudmundsson, M. Simons, *Journal of Glaciology* **64**, 583 (2018).

59. F. S. Graham, M. Morlighem, R. C. Warner, A. Treverrow, *The Cryosphere* **12**, 1047 (2018).

60. R. Alley, J. Perepezko, C. Bentley, *Journal of Glaciology* **32**, 425 (1986).

61. P. Duval, O. Castelnau, *Journal de Physique IV* **5**, 197 (1995).

62. P. Duval, M. F. Ashby, I. Anderman, *Journal of Physical Chemistry* **87**, 4066 (1983).

63. N. J. Austin, B. Evans, *Geology* **35**, 343 (2007).

64. N. Azuma, T. Miyakoshi, S. Yokoyama, M. Takata, *Journal of Structural Geology* **42**, 184 (2012).

65. P. Duval, *Annals of Glaciology* pp. 3–6 (1985).

66. R. Alley, J. Perepezko, C. Bentley, *Journal of Glaciology* **32**, 425 (1986).